RSC Advances

RSC Advances

www.rsc.org/advances

ROYAL SOCIETY OF CHEMISTRY

www.rsc.org/advances

RSC Advances

COMMUNICATION

Biomimetic Graphene Oxide-Hydroxyapatite Composites *via* in situ Mineralization and Hierarchical Assembly

Yaling Li,[a] ‡ Cuilian Liu,[a] ‡ Halei Zhai,[a] Genxing Zhu,[a] Haihua Pan,[ab] Xurong Xu[ab] and Ruikang Tang*[ab]

Graphene oxide-hydroxyapatite hybrid is synthesized *via* in situ mineralization. The integrated HAP nanoplates share the similar size, morphology and orientations with those in natural bones. With the excellent mechanical property and
10 **biocompatibility, the composites offer potential application in load-bearing bone repair, scaffold material, and alternative model for biomimetic research.**

Nature has created various excellent materials during the process of evolution. The huge diversity of elaborate hierarchical
15 structures existing in biological systems is increasingly becoming a source of inspiration for scientists to design advanced materials.[1] These biominerals are usually integrated organic-inorganic hybrids with distinguished mechanical properties, which are quite distinct from individual components. Despite of
20 the highly controlled hierarchical structures, another common feature is that the biominerals often involve nanocrystals as building block arranged in high order with organic molecule as the supporting matrix.[2] For example, bone is mainly composed of ultrathin plate-like hydroxyapatite (HAP) nanocrystals (2-5 nm in
25 thickness) and collagen, in which HAP crystals are parallel aligned and tightly interact with the collagen fibers.[3] As one of the most remarkable materials in nature, bone usually serves as an elastic structural frame and internal organ protection in body (with modulus about 10 to 20 GPa[4, 5]). The nanoscale feature of
30 bone minerals can confer the optimum strength and the maximum tolerance of flaws on the tissues.[2] Although there have been a mass of researches on fabrication of bone-like composites,[6, 7] the artificial design of materials mimicking bone both in structure and mechanical property still remains a great challenge.
35 Biominerals in tissues are usually formed under the control of macromolecular templates of proteins, peptides, and polysaccharides.[8-10] During the mineralization process, the organic matrixes are required to provide not only mechanical support but also effective control over minerals crystal nucleation
40 and growth to obtain highly ordered deposition and integration.[11] Accordingly, the organic templates are desired to possess the advantages of localized nucleation and ordered assembly at nanoscale. Graphene, a single layer of carbon atoms tightly packed into a honeycomb lattice, has attracted tremendous
45 attention for its remarkable physical properties.[12] Graphene oxide (GO), one of the most important derivatives of graphene, can be considered as consisting of graphene sheets decorated with

hydrophilic oxygen functional groups (hydroxyl, epoxide, and carboxyl group).[13] Accordingly, it can act as a useful building
50 block for versatile functional materials synthesis. Various GO-based composites with specific functions have been reported,[14] especially for medical and biological applications, such as tissue engineering,[15] drug delivery,[16] cellular imaging,[17] biosensor,[18] and antibacterial materials.[19] However, the previous in vitro and
55 in vivo studies show that GO might become a health hazard.[20] GO can be internalized by cells, and then escape from subcellular compartments, travel within the cytoplasm, and translocate into the nucleuses.[21] To adjust the cytotoxicity, biomacromolecules such as chitosan,[16] gelatin,[22] Tween,[23] have been used to modify
60 GO sheets so as to alleviate the potential risks. Biominerals, like HAP, exhibiting excellent biocompatibility, have also been suggested to composite with GO to improve weak mechanical properties of the pure HAP as well as reducing the toxicity of GO.[24, 25] However, we note that the reported fabrication methods
65 are relatively complicated or time consuming, and specific macromolecules are usually required to pre-modify the GO sheets. More importantly, the uncontrolled precipitation process of calcium phosphate on GO surface usually leads to random and weak combination between HAP and GO sheets.
70 In this work, we directly used GO as a mineralization substrate and reinforce component to produce the biomimetic GO-HAP composites *via* a facile one-step in situ crystallization method. GO could be considered as a two-dimensional (2-D) hydrophilic macromolecule[26] with abundant mineralization related groups
75 (hydroxyl, and carboxyl group). The unique 2-D geometry of GO could regulate the inorganic phase deposition onto the surface of GO.[27] With pricise control of mineralization, plate-like HAP could nucleate and growth on GO surface. These HAP plates tightly bind with GO with their (100) face. Thus, it was rather
80 readily to obtain parallel arrangement at 3-D scale as the layered stack and assembly of the GO sheets.[28] Via a vacuum assisted self-assembly process, a GO-HAP paper would be easily obtained, in which the plate-like nanocrystals were in parallel arrangement on GO. Accordingly, the elastic modulus of the resulted paper
85 could be comparable to modules of natural bone and the resulted composite material exhibited excellent biocompatibility.
GO was prepared from pristine graphite by a modified Hummers and Offema method.[29] GO and calcium chloride were dispersed in ethylene glycol-water mixture solvent (170 ml
90 ethylene glycol and 30 ml water), followed by ultrosonication for 30 min. Afterwards, disodium hydrogen phosphate aqueous

COMMUNICATION
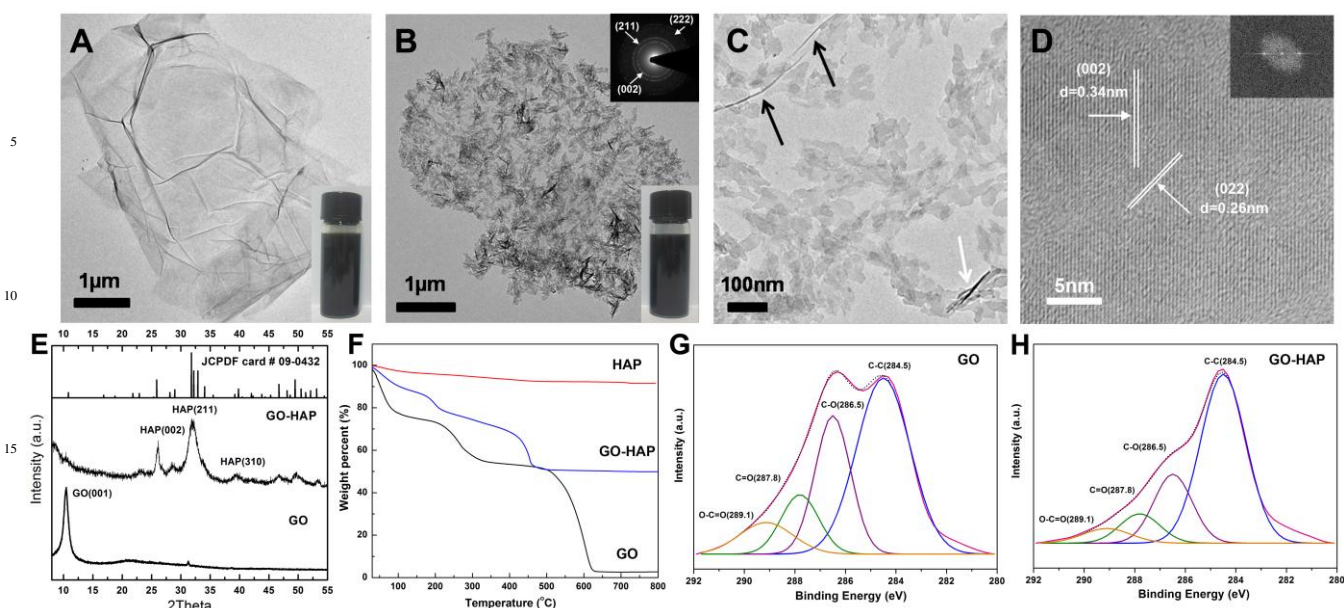
Figure 1. TEM images of GO(A) and GO-HAP (B and C) composites, inset in B (left, up) is selected area electron diffraction (SAED) pattern. Both GO and GO-HAP showed good dispersity in water. (D) HRTEM image of HAP nanoplates on GO sheets, inset was the FFT image of crystal lattice. (E) XRD patterns of GO and GO-HAP powder samples. (F) TGA profiles of GO-HAP , GO and HAP. (G) and (H) XPS analysis of the C1s region in GO and GO-HAP. A large loss of oxygen-functional groups after a one-step synthesis procedure is evident.

solution was added to initiate the in situ mineralization of calcium phosphate on GO sheets and the reaction was kept at $85\pm1^{o}C$ for 12 h to accelerate the mineralization process. Under transmission electron microscopy (TEM), the GO sheets were multilayers with size of a few micrometers (Figure 1A). After the mineralization process (Figure 1B), the GO surfaces were covered by the newly formed nanoplates, which were typically tens of nanometers in length and width (Figure 1C). The thickness of HAP plate was several nanometers by measuring the standing ones (Figure 1C, white arrows), which might be induced by the wrinkle or the fold of GO (Figure 1C, black arrows). A direct measurement by atomic force microscopy (AFM, Figure S1) also confirmed that the thickness of the plates was 4.12 ± 0.52 nm. The strong diffraction ring in selected area electron diffraction (SAED, Figure 1B) could be assigned to the (002), (211) and (222) planes of HAP. The Ca/P ratios determined by energy dispersive spectroscopy analysis (EDS, Figure S2) were about 1.676 and the value was consistent with the stoichiometric ratio of Ca/P in HAP. HRTEM image (Figure 1D) showed that the exposed surface of HAP nanoplates was (100) planes, indicating that the HAP nanoplates bind with GO by the (100) planes. X-Ray Diffraction patterns (XRD, Figure 1E) further demonstrated the formation of HAP. The XRD peaks at 25.9^{o}, 31.8^{o} and 39.8^{o} were indexed to the (002), (211) and (310) of HAP (JCPDF card # 09-0432), respectively. The strong and sharp peak of GO at $2\theta=10.44^{o}$ indicate the (001) interlayer spacing of 0.85nm and AFM examination showed that GO sheets had a thickness of 0.97 ± 0.39 nm. This value was much larger than that of pristine graphite

(0.34 nm) due to the introduction of oxygen-containing functional groups on the graphite sheets.[30] However, after the mineralization, the (001) reflection peak of layered GO almost disappeared, which was consistent with previous studies that the diffraction peaks became weakened or even disappear whenever the regular stacks of GO sheets were exfoliated.[31] Further, the small differences between GO and GO-HAP in the Raman study (Figure S3) indicated that the GO was not thoroughly reduced to graphene during the mineralization.[32] The weight ratio of HAP/GO in composites was 2.12 from TGA results (Figure 1F, the influence of adsorbed water was eliminated). The initial weight loss around $100^{o}C$ in the samples was due to the evaporation of absorbed water. Around $250^{o}C$, there was an obvious weight loss in GO and GO-HAP, which was attributed to the decomposition of the residual oxygen-containing groups. The sharp weight loss above $450^{o}C$ was caused by the thermal decomposition of GO.[25] Notably, the weight percents of inorganic and organic components in GO-HAP composites (HAP, 67.9%, GO, 32.1%) were quite similar to that of bone, in which the mineral part contributes with 65-70% to the tissue and the organic part, 25-30%.[3] X-ray photoelectron spectroscopy (XPS) was conducted to further investigate the chemical compositions of samples. High-resolution C1s spectra of GO and GO-HAP (Figures 1G and 1H) showed that four different types of carbon components were existed: C-C (284.5 eV), C-O(C-OH) (286.5 eV), C=O (287.8 eV) and O-C=O (289.1 eV). Although some
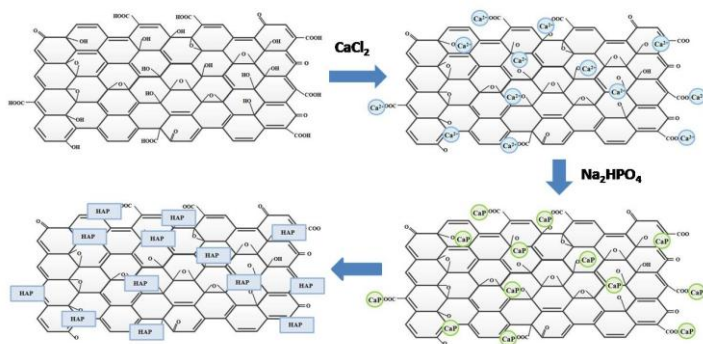
Scheme 1. The proposed in suit mineralization mechanism of HAP on GO sheets. CaP: crystal nucleus formed on GO sheets, HAP: HAP
10 nanoplates.

oxygen-containing groups remained in GO-HAP, the peak intensities were much weaker in comparison with pure GO. These phenomena indicated that GO was partially deoxygenated during the mineralization process, which was mainly caused by the
15 reduction process with ethylene glycol.[31]

To further investigate the formation process of the GO-HAP composites, various samples were separated from the reaction mixture at different time intervals, and then were observed under TEM (Figure S4). The samples, with a short reaction time for
20 2min, were GO sheets with disordered precursors (small pieces of several nanometres, Figure S4A) on their surfaces, which were confirmed as poorly crystallized minerals (Figure S5). With the reaction proceeding from 1 to 4 h, the nanoplates on GO sheets gradually grew up and spread on GO surface. After 8 h, the
25 crystal growth was completed and the surfaces of GO sheets were covered with HAP nanoplates. The increasing of crystallinity of the deposited HAP minerals with the reaction time could be revealed by XRD (Figure S5). Scheme 1 demonstrates a possible formation mechanism of the as-obtained GO-HAP composites. It
30 was known that GO sheets were decorated with abundant oxygen-containing groups, especially hydroxyl and carboxyl groups.[13] These functional groups acted as anchor sites and enabled in situ formation of HAP mineral phase on the surfaces of GO sheets. In the initial stage, calcium ions, formed by the
35 dissolution of $CaCl_2$ in ethylene glycol and water, favourably bounded with these oxygen-containing groups. With the addition of Na_2HPO_4 aqueous solution, a large number of nuclei formed on GO sheets to induce HAP crystallization. The morphology of HAP crystals was related to the specific EG-water mixed solvent.
40 In this system, EG provided a medium for the controlled release of free calcium and phosphate ions from their electrolyte solids, which would possibly reduce the driving force of homogeneous nucleation and promote HAP growing on GO substrates.[54] It was found that similar plate-like HAP crystals also formed without
45 GO (Figure S6). We noted that the water content determined the mineralization process of HAP on GO surface. The less water content would slow down the deposition process and obtained HAP with less crystallinity (Figure S7). Accordingly, with simple control of mixture solvent, HAP nanoplates could precisely form
50 on GO surface with heterogeneous crystallization. In this process,

the in situ mineralization was a key to achieve the structured GO-HAP complex. In order to exclude free HAP nanoplates attached on GO sheets, as-synthesized HAP nanoplates were added into reaction solution instead of ions precursors (Ca^{2+} and HPO_4^{2-}).
55 After 12 h, TEM images (Figure S8A) showed that there were some HAP crystals sparsely covering on GO sheets, but after ultrasonication (40 kHz, 180 W, 25°C) for 2 h (Figure S8B), the crystals became visibly less. In contrast, after the same ultrasonic treatment, GO-HAP composites underwent almost no obvious
60 change and there were nearly no scattered HAP nanoplates found (Figure S8C). It followed that the HAP crystals were rooted on the GO sheets, which could be understood as the integration of HAP and GO phases by the hydrophilic groups on sheets during the in situ mineralization process.
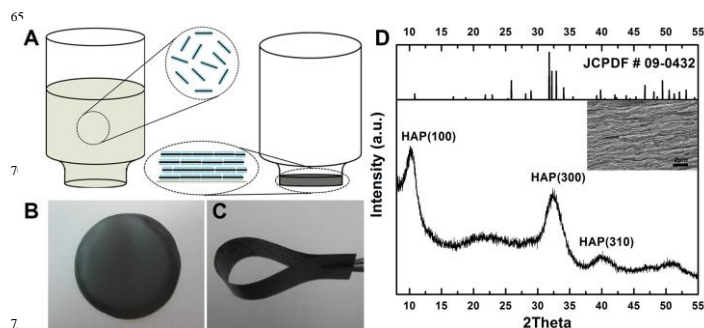
Figure 2. (A) Self-assembly process of GO-HAP sheets during vacuum filtration. (B) and (C) Digital photograph of GO-HAP paper. (D) XRD pattern of the GO-HAP paper. In comparison with Figure 1D, the (002) reflection disappears in the paper-like assembly. Inset is SEM image of
80 fracture section of GO-HAP paper, revealing the lamellar structure.

It has been demonstrated that the apatite nanocrystals can provide the organic-inorganic nanocomposite in biological bone with the favorable mechanical properties.[2, 33] We noted that the dimensions of the resulted HAP nanoplates on GO sheets were
85 fairly similar to those in bone tissues.[3] The GO-HAP composite could be constructed into a well-ordered macroscopic structure with the bone-like features for a mechanical examination. The resulted GO-HAP sheets were well-dispersed in water (inset in Figure 1B) and could be self-assembled into a paper-like material
90 under a directional flow.[28] In the present work, we got a free-standing paper *via* vacuum filtration of colloidal dispersions of the GO-HAP sheets (Figure 2A). Figures 2B and 2C showed that the obtained paper was uniform, complete and flexible. SEM image (inset in Figure 2D) of the fracture surface of the GO-HAP
95 paper revealed the lamellar structure within the bulk material. Notably, XRD pattern of the GO-HAP paper (Figure 2D) displayed that (002) plane reflection (25.9^o) of HAP disappeared, while the reflection of (100) and (300) planes (10.8^o, and 32.9^o, respectively) got evident enhancements. By using the software of
100 PeakFit v4.12, the peaks of (211), (112) and (300) in XRD patterns of GO-HAP powder and paper samples (Figure S9) were separated to calculate the peak area ratio of (300) to (002) planes (shown as $I_{(300)/(002)}$). $I_{(300)/(002)}$ of powder sample was only 1.02, while the value for paper sample was 29.41. Such a significant
105 difference between GO-HAP powder and paper samples (Figure 1E, Figure 2D) was attributed to the unique orientation of HAP

nanoplates on GO sheets and the subsequent orderly assembly. It was indicated by HRTEM (Figure 1D) that the plate-like HAP crystals were integrated with GO sheets *via* (100) face, and packed into high ordered lamellar structure in our GO-HAP paper. Moreover, due to the 2-D geometry of GO, not only the HAP nanoplates, but also all their (100) planes were approximately parallel to each other. The unique structure resulted in the obvious enhancement of (300) reflection and disappearance of (002) reflection.[55] In biological bone, the ultrathin HAP nanoplates are oriented along the long axes of the collagen fibrils with their (100) planes parallel to each other.[34] Therefore, the GO-HAP paper shared the similar hybrid structure with that of natural bone.
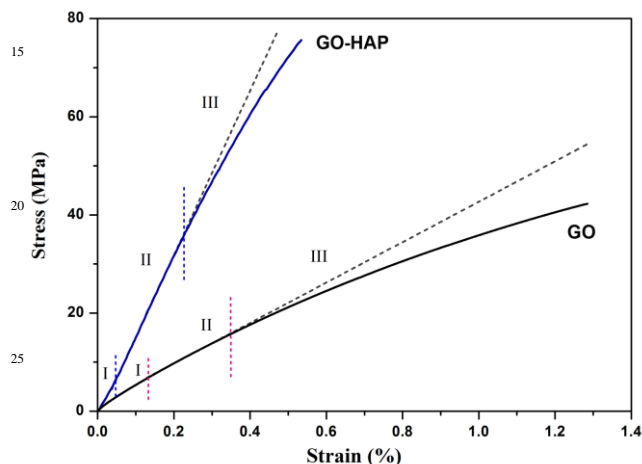
Figure 3. Stress-strain curves of GO-HAP and GO papers.

	E_I [GPa]	E_{II} [GPa]	σ [MPa]	ε [%]	U [KJ/m^3]
Bone	10-20 [4, 5]		89-114 [51]	1.1-2.5 [52]	120-875 [53]
HAP	5.18-5.92 [25]		/	/	/
GO paper	4.2	5.1	42.3	1.28	313.6
GO-HAP paper	13.6	16.9	75.6	0.53	214.9

EI = modulus in the initial region; EII = modulus during the "linear" part; σ = ultimate strength; ε = ultimate strain; U = work of fracture.

Table 1. Mechanical properties of bone, HAP, GO and GO-HAP papers. Note: For HAP powder, it is very difficult to obtain the tension-stress curve to calculate the values of tensile strength, strain and work of fracture for bulk HAP powders.

This unique structure of highly ordered nanoplates embedded in the relatively soft GO matrix would lead to an optimal mechanical performance. Typical stress-strain curves of GO-HAP and GO papers were shown in Figure 3. Three regimes of deformation were observed: straightening, almost linear ("elastic"), and plastic.[28] The initial modulus (E_I) of GO-HAP paper was 13.6GPa, which was 223% higher than that of unmodified GO paper (4.2GPa), indicating that GO-HAP paper was significantly stiffer than the pure GO one against the initial loading (Table 1). It was proposed that the initial tensile load can lead to structural sliding of GO sheets to overcome physical

wrinkling or "waviness" that resulted from the fabrication process and thus to achieve the best interlocking geometry.[35] Correspondingly, the modulus continued to increase as the samples straightened and entered the linear region. The modulus (E_{II}) of GO-HAP paper during the linear part was 16.9GPa, 231% higher than the GO paper (5.1GPa). The modulus of our GO-HAP paper were higher than reported modulus values for bucky paper (<10GPa),[36] graphite foil (~5GPa),[37] and paper-like materials (~5-15GPa)[22, 38, 39]. The tensile strength (σ) of GO-HAP paper was 75.6MPa, 78% higher than the GO paper. However, the GO-HAP paper underwent a reduction of toughness due to the integration of the rigid HAP crystals. The ultimate strain (ε) and fracture toughness (U) of GO-HAP paper were 0.53%, 214.9kJ/m^3, while these values for GO paper were 1.28%, 313.6kJ/m^3, respectively. Nevertheless, compared with the current used cross-linking agents to fabricate GO-based composites such as polyallylamine (GO-PAA, 0.32%, 180kJ/m^3),[40] poly(vinyl alcohol) (GO-PVA, 0.27%, 100kJ/m^3),[41] glutaraldehyde (GO-GA, 0.4%, 200kJ/m^3),[42] or borate (GO-borate, 0.15%, 140kJ/m^3),[43] GO-HAP paper here was more tougher. These results indicated that the HAP nanoplates played a pivotal role in retaining toughness as the stiffness increased, which were both equally important in load-bearing materials design.

The improvement of mechanical strength was originated from the ordered GO-HAP layered structure at nanoscale. Under tensile stress, the deformation mechanism was similar as a staggered model of load transfer in bone matrix.[33] It was shown that as soon as the structural size reaches the critical length (the size of fracture process zone), materials become insensitive to flaws.[2] Thus, the nanometer size of the mineral crystals in biocomposites became important to ensure the optimum fracture strength and maximum tolerance of flaws. More importantly, the effective load transfer between minerals and soft matrix also played a key role in damage shielding.[44] As previously mentioned, the binding force between GO sheets and HAP nanoplates were strong, mainly resulted from the high specific surface areas and in suit crystallization process. In the composite, the HAP crystal orientations were induced and controlled by the GO substrates during the in situ mineralization. And the resulted GO-HAP sheets could be further self-assembled to form the free-standing paper with the lamellar structure. When the GO-HAP paper was exposed to an applied tensile stress, the load could be transferred by soft GO sheets via shear between rigid HAP plates. Since HAP crystals could bear most of stress, the strength of the hybrid material was significantly improved.

Recently, repair of load-bearing defects resulting from disease or trauma becomes a critical problem for bone tissue engineering.[45] HAP, for its excellent biocompatibility, has been extensively studied for this application. However, the conventionally synthesized HAP crystallites cannot have sufficient mechanical strength to repair these defects directly, therefore, have been limited to the non-load-bearing applications.[41, 45] After composite with GO, the mechanical properties of the resulted GO-HAP composites (Table 1) were greatly improved. Compared with some bone tissues, the elastic modulus of GO-HAP paper was higher than that of the mineralized collagen fibers (3-7GPa),[46] rat vertebra (11-

13GPa),[47] bovine distal femora (9-12GPa),[4] red deer anthler (7-8GPa),[48] and comparable to human femur bone (13-15GPa),[49] and human tibia bone (13-16GPa).[50] Accordingly, with the comparable stiffness to that of bones, the GO-HAP composite
5 showed promising application in bone tissue engineering.

Figure 4. (A) Relative cell viability of human osteosarcoma cells (MG-63) treated with GO, GO-HAP and conventional HAP at various concentrations, and fluorescent images of MG63 cells cultured on
25 (B)glass, (C)GO, (D)conventional HAP and (E)GO-HAP films for 24 h.

Different from GO, the GO-HAP composites were also featured by their excellent biocompatibility. In vitro cytotoxicity test (MTT assay) was conducted to evaluate the GO-HAP material for its potential application in biomedicine and
30 bioengineering. Human osteosarcoma cells (MG63), a representative of human osteoblast-like cell, were used in this biological assessment. As shown in Figure 4A, GO had an unneglectable toxicity on MG63 cells, presenting a dose-dependent cytotoxic effect. At the highest concentration (200mg
35 L^{-1}), only 52% of the cells remain viable. However, after modified by HAP crystals, the toxicity of GO was reduced remarkably. Even after 24h exposure to the GO-HAP hybrid materials, the relative cell viability could keep at a high level of 81-88% and these values were almost unaffected by the material
40 concentrations. In the parallel experiment, we selected the conventional HAP to repeat the experiment. As expected, HAP had relatively high cell viability (88-94%) under all applied concentrations. These results revealed that after modification with HAP, the biocompatibility of GO had been significantly
45 enhanced, which could be comparable to the HAP biomineral. The cell attachment and morphology on these different substrates had also been examined and the glass was used as blank control. The fluorescent staining images (Figures 4B-4E) showed that the cell density increased from GO film, to GO-HAP film, to HAP
50 film, which was consistent with MTT results. Most cells on the films and glass were well-spread and exhibited an elongated and highly branched morphology, revealing that cells were well adhered on substrates. However, compared to GO-HAP film, cells on GO film were rather less, revealing the poor
55 biocompatibility of GO. After the mineralization modification, the cell toxicity of GO could be markedly reduced by the high

coverage percentages and well-ordered orientation of HAP crystals. Thus, the developed GO-HAP composite shared the similar structure, mechanical strength and bioactivity with the
60 natural bone, which could be specifically suitable for the load-bearing substitution.

Conclusions

In summary, we synthesized GO-HAP composites via biomimetic in situ mineralization and they can assembly into the
65 highly ordered bone-like structure. The tensile strength and Young's modulus of the GO-HAP paper can achieve the optimal level of the biological bone and the material also possesses the excellent biocompatibility. Since the GO-HAP composites mimic natural bone in both structure and function, we suggest that the
70 GO-HAP composites may offer a potential in bone tissue repair and an alternative research model for biomimetic bone.

Acknowledgements

Notes and references

80 [a] *Center for Biomaterials and Biopathways, Department of Chemistry, Zhejiang University, Hangzhou, China. Fax: (+)86 571 87953736; Tel: (+)86 571 87953736; E-mail: rtang@zju.edu.cn*
[b] *Qiushi Academy for Advanced Studies, Zhejiang University, Hangzhou, China.*
85 † Electronic Supplementary Information (ESI) available: [details of any supplementary information available should be included here]. See DOI: 10.1039/b000000x/
‡ These authors contributed equally to the work.

90 1. S. Mann, Biomineralization: principles and concepts in bioinorganic materials chemistry, Oxford University Press, Oxford, 2001.
2. H. Gao, B. Ji, I. L. Jager, E. Arzt and P. Fratzl, Proc. Natl. Acad. Sci. U. S. A., 2003, **100**, 5597-5600.
3. C. J. N. Liam C. Palmer, Stuart R. Kaltz, Erik D. Spoerke, Samuel I.
95 Stupp, Chem. Rev., 2008, **108**, 4754-4783.
4. R. B. Ashman and R. Jae Young, J. Biomech., 1988, **21**, 177-181.
5. J.-Y. Rho, L. Kuhn-Spearing and P. Zioupos, Med. Eng. Phys., 1998, **20**, 92-102.
6. E. D. Spoerke, S. G. Anthony and S. I. Stupp, Adv. Mater., 2009, **21**,
100 425-430.
7. A. M. Collins, N. J. V. Skaer, T. Gheysens, D. Knight, C. Bertram, H. I. Roach, R. O. C. Oreffo, S. Von-Aulock, T. Baris, J. Skinner and S. Mann, Adv. Mater., 2009, **21**, 75-78.
8. R. Lakshminarayanan, R. M. Kini and S. Valiyaveettil, Proc. Natl.
105 Acad. Sci. U. S. A., 2002, **99**, 5155-5159.
9. Y.-Y. Hu, A. Rawal and K. Schmidt-Rohr, Proc. Natl. Acad. Sci. U. S. A., 2010, **107**, 22425-22429.
10. J. Aizenberg, G. Lambert, S. Weiner and L. Addadi, J. Am. Chem. Soc., 2001, **124**, 32-39.
110 11. S. Weiner, W. Traub and S. B. Parker, Phil. Trans. R. Soc. B, 1984, **304**, 425-434.
12. A. K. Geim and K. S. Novoselov, Nat. Mater., 2007, **6**, 183-191.
13. D. R. Dreyer, S. Park, C. W. Bielawski and R. S. Ruoff, Chem. Soc. Rev., 2010, **39**, 228-240.
115 14. X. Huang, X. Qi, F. Boey and H. Zhang, Chem. Soc. Rev., 2012, **41**, 666-686.

15. S. H. Ku, M. Lee and C. B. Park, Adv. Healthc. Mater, 2013, **2**, 244-260.
16. H. Bao, Y. Pan, Y. Ping, N. G. Sahoo, T. Wu, L. Li, J. Li and L. H. Gan, Small, 2011, **7**, 1569-1578.
17. Y. Wang, W. C. Lee, K. K. Manga, P. K. Ang, J. Lu, Y. P. Liu, C. T. Lim and K. P. Loh, Adv. Mater., 2012, **24**, 4285-4290.
18. Y. Liu, D. Yu, C. Zeng, Z. Miao and L. Dai, Langmuir, 2010, **26**, 6158-6160.
19. W. Hu, C. Peng, W. Luo, M. Lv, X. Li, D. Li, Q. Huang and C. Fan, ACS Nano, 2010, **4**, 4317-4323.
20. K. H. Liao, Y. S. Lin, C. W. Macosko and C. L. Haynes, ACS Appl. Mater. Interfaces, 2011, **3**, 2607-2615.
21. A. Bianco, Angew. Chem. Int. Ed., 2013, **52**, 4986-4997.
22. C. Wan, M. Frydrych and B. Chen, Soft Matter, 2011, **7**, 6159.
23. S. Park, N. Mohanty, J. W. Suk, A. Nagaraja, J. An, R. D. Piner, W. Cai, D. R. Dreyer, V. Berry and R. S. Ruoff, Adv. Mater., 2010, **22**, 1736-1740.
24. S. Kim, S. H. Ku, S. Y. Lim, J. H. Kim and C. B. Park, Adv. Mater., 2011, **23**, 2009-2014.
25. M. Li, Y. Wang, Q. Liu, Q. Li, Y. Cheng, Y. Zheng, T. Xi and S. Wei, J. Mater. Chem. B., 2013, **1**, 475.
26. L. J. Cote, F. Kim and J. Huang, J. Am. Chem. Soc., 2008, **131**, 1043-1049.
27. S. Chen, J. Zhu, X. Wu, Q. Han and X. Wang, ACS Nano, 2010, **4**, 2822-2830.
28. D. A. Dikin, S. Stankovich, E. J. Zimney, R. D. Piner, G. H. B. Dommett, G. Evmenenko, S. T. Nguyen and R. S. Ruoff, Nature, 2007, **448**, 457-460.
29. W. Chen and L. Yan, Adv. Mater., 2012, **24**, 6229-6233.
30. C. Xu, X. Wu, J. Zhu and X. Wang, Carbon, 2008, **46**, 386-389.
31. C. Xu, X. Wang and J. Zhu, J. Phys. Chem. C, 2008, **112**, 19841-19845.
32. K. N. Kudin, B. Ozbas, H. C. Schniepp, R. K. Prud'Homme, I. A. Aksay and R. Car, Nano Lett., 2008, **8**, 36-41.
33. H. S. Gupta, J. Seto, W. Wagermaier, P. Zaslansky, P. Boesecke and P. Fratzl, Proc. Natl. Acad. Sci. U. S. A., 2006, **103**, 17741-17746.
34. M. J. Olszta, X. Cheng, S. S. Jee, R. Kumar, Y.-Y. Kim, M. J. Kaufman, E. P. Douglas and L. B. Gower, Mater. Sci. Eng. R. Rep., 2007, **58**, 77-116.
35. S. Park, K.-S. Lee, G. Bozoklu, W. Cai, S. T. Nguyen and R. S. Ruoff, ACS Nano, 2008, **2**, 572-578.
36. X. Zhang, T. Sreekumar, T. Liu and S. Kumar, The Journal of Physical Chemistry B, 2004, **108**, 16435-16440.
37. M. Dowell and R. Howard, Carbon, 1986, **24**, 311-323.
38. D. Zhong, Q. Yang, L. Guo, S. Dou, K. Liu and L. Jiang, Nanoscale, 2013.
39. Y. Xu, W. Hong, H. Bai, C. Li and G. Shi, Carbon, 2009, **47**, 3538-3543.
40. S. Park, D. A. Dikin, S. T. Nguyen and R. S. Ruoff, J. Phys. Chem. C, 2009, **113**, 15801-15804.
41. K. W. Putz, O. C. Compton, M. J. Palmeri, S. T. Nguyen and L. C. Brinson, Adv. Funct. Mater., 2010, **20**, 3322-3329.
42. Y. Gao, L.-Q. Liu, S.-Z. Zu, K. Peng, D. Zhou, B.-H. Han and Z. Zhang, ACS Nano, 2011, **5**, 2134-2141.
43. Z. An, O. C. Compton, K. W. Putz, L. C. Brinson and S. T. Nguyen, Adv. Mater., 2011, **23**, 3842-3846.
44. B. Ji and H. Gao, J. Mech. Phys. Solids, 2004, **52**, 1963-1990.
45. A. J. Wagoner Johnson and B. A. Herschler, Acta Biomater., 2011, **7**, 16-30.
46. F. Yuan, S. R. Stock, D. R. Haeffner, J. D. Almer, D. C. Dunand and L. C. Brinson, Biomech. Model. Mechanobiol., 2011, **10**, 147-160.
47. E. Hamed, I. Jasiuk, A. Yoo, Y. Lee and T. Liszka, J. R. Soc. Interface, 2012, **9**, 1654-1673.
48. J. Currey, T. Landete-Castillejos, J. Estevez, F. Ceacero, A. Olguin, A. Garcia and L. Gallego, J. Exp. Biol, 2009, **212**, 3985-3993.
49. P. K. Zysset, X. Edward Guo, C. Edward Hoffler, K. E. Moore and S. A. Goldstein, J. Biomech., 1999, **32**, 1005-1012.
50. J. Y. Rho, R. B. Ashman and C. H. Turner, J. Biomech, 1993, **26**, 111-119.
51. M. Akao, H. Aoki and K. Kato, J. Mater. Sci., 1981, **16**, 809-812.
52. D. L. Kopperdahl and T. M. Keaveny, J. Biomech., 1998, **31**, 601-608.
53. P. Zioupos and J. D. Currey, Bone, 1998, **22**, 57-66.
54. J. Tao, W. Jiang, H. Zhai, H. Pan, X. Xu, R. Tang, Cryst. Growth Des., 2008, **8**, 2227-2234.
55. Z. Zhuang and M. Aizawa, J. Mater. Sci.: Mater. Med., 2013, **24**, 1211-1216.

Biomimetic Graphene Oxide-Hydroxyapatite Composites via in situ

Mineralization and Hierarchical Assembly

Yaling Li, Cuilian Liu, Halei Zhai, Genxing Zhu, Haihua Pan, Xurong Xu, and Ruikang Tang*
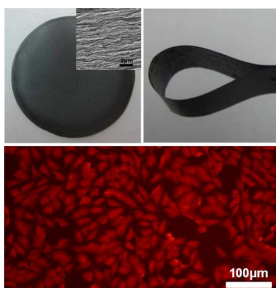
Graphene oxide(GO)-hydroxyapatite(HAP) hybrid with the excellent mechanical property and biocompatibility is synthesized via in situ mineralization and hierarchical assembly.